How the utilised SOC window in commercial Li-ion pouch cells influence battery ageing

Journal of Power Sources Advances 8 (2021) 100054

Contents lists available at ScienceDirect

Journal of Power Sources Advances

journal homepage: www.journals.elsevier.com/journal-of-power-sources-advances

How the utilised SOC window in commercial Li-ion pouch cells influence battery ageing

Evelina Wikner [a,*], Erik Björklund [b], Johan Fridner [c], Daniel Brandell [b], Torbjörn Thiringer [a]

[a] Department of Electric Power Engineering, Electrical Machines and Power Electronics, Chalmers University of Technology, SE-412 96, Göteborg, Sweden
[b] Department of Chemistry-Ångström Laboratory, Uppsala University, Box 538, 75121 Uppsala, Sweden
[c] Volvo Car Corporation, SE-412 96, Göteborg, Sweden

ARTICLE INFO

Keywords:
Lithium-ion battery
Battery ageing
State of charge window
Cycle life
Ageing mechanism

ABSTRACT

In many lithium-ion battery (LIB) applications, e.g. hybrid vehicles and load-levelling storage systems, only part of the state-of-charge (SOC) range needs to be utilised. This offers the possibility to use an optimal SOC window to avoid LIB ageing. Here, a large test matrix is designed to study LIB ageing in a commercial 26 Ah pouch cell, in order to map the ageing behaviour at different SOC levels with respect to temperature and current. A quantification of the degradation modes, loss of lithium inventory (LLI), loss of active positive (LAM_{PE}) and negative (LAM_{NE}) electrode materials is made by analysing the change in the open circuit voltage (OCV). A key result is that lower SOC intervals significantly improved battery ageing. Even during harsh test conditions, such as high C-rates and temperatures, the cells deliver more than three times the expected number of full cycle equivalents. High SOC combined with high C-rate increase ageing where the dominating ageing mechanisms are LLI, followed by LAM_{PE}.

1. Introduction

The established knowledge is that Lithium-ion batteries (LIB) degrade faster when operated at either high or low state of charge (SOC), high temperature and high C-rate [1–8]. It has also been shown that using a limited part of the available SOC window, which is applicable in applications such as hybrid vehicles and stationary battery storages for load-levelling, improves the battery lifetime [9–11].

Lifetime testing of large, high-quality vehicle batteries is very expensive and time consuming. Therefore, there exist only a few studies on limited SOC intervals on smaller commercial cylindrical cells [7,11].

Post mortem (PM) analysis is the main method used to characterise LIB ageing mechanisms. However, this requires a material lab facility with advanced equipment and several time consuming analysis methods [12]. Various mathematical and non-invasive approaches have been developed to make use of the characteristics in the potential curve [4, 13–18].

In this study, we focus on investigating ageing in high-quality automotive pouch cells. The purpose is to quantify the impact of SOC, C-rate and temperature on the ageing of this type of commercial LIB cells. The test matrix was designed to study the ageing as a function of SOC, C-rate and temperature; 10% of the battery capacity was utilised at 7 different SOC intervals, 3 C-rates and 3 temperatures. The cells were cycled for up to 28 months.

PM analysis was conducted on a selected number of the investigated cell to analyse the ageing mechanisms and, complementary, the changes in the potential curves were used to estimate and quantify the loss of active materials and lithium inventory.

2. Test set-up

The battery test equipment used were Maccor Series 4000, PEC SBT0550 and Digatron MCT 100-05-8. All tests were performed in a temperature controlled environment using a Vötsch VT3 7034, as well as a VT3 4060 and a Climate Temperature System, T-40/350. The temperatures were set to 25, 35 or 45 °C.

47 commercial 26 Ah pouch cells were tested using constant current (CC) cycles as shown in Table 1. The ageing was performed during a 4 year period, where the longest single test duration was 2.4 years. The cells came from two different batches, but the standard deviation in initial capacity (0.23%) and resistance (2.3%) were small (suppl. Fig. S1). The ambition was to have two cells for each test case, however, the results for duplicates tests demonstrate an excellent reproducibility of this commercial cell. With a limited number of channels available, a decision

* Corresponding author.
E-mail address: evelina.wikner@chalmers.se (E. Wikner).

https://doi.org/10.1016/j.powera.2021.100054
Received 5 November 2020; Received in revised form 5 March 2021; Accepted 6 March 2021

Table 1
Test matrix for lifetime cycling. Designation I and II indicates one or two tested cells and the superscripts refer to cells subjected to PM analysis, * using CC-CV@4.06 V, and ** CC with maximum 4.25 V.

Symmetric	T = 25 °C			T = 35 °C			T = 40–45 °C		
cycles, SOC [%]	±1C	±2C	±4C	±1C	±2C	±4C	±1C	±2C	±4C
0–10		II			I			II	
10–20	I	I	I	I	I	II	I	II^{PM}	II^{PM}
20–30		I						II	
30–40									
40–50		I			I			I	
50–60									
60–70	I	I	II	I^{PM}	I	II^{PM}	I	II^{PM}	I
70–80		I						II	
80-90**		I						I	
80–90*		I						I	
10–90*		I						I	
0–90*		I^{PM}			I			I^{PM}	

was taken to use single cells for an expanded matrix. The 47 cells were selected from a larger test matrix; the complete compilation of results can be found in Refs. [19,20].

The cell capacity is here defined by a voltage interval, where 2.8 V correspond to 0% SOC and 4.15 V to 100% SOC. The voltage interval being defined by the cell manufacturer. The cells use an organic electrolyte with 1 M $LiPF_6$, a negative electrode (NE) of natural graphite and a positive electrode (PE) which employs a mixture of lithium manganese oxide (LMO) and lithium nickel manganese cobalt oxide (NMC).

Testing was conducted with CC cycles in 90, 80 and 10% SOC intervals. For the tests in 10% SOC intervals, a small drift in SOC interval could be noticed after 500 cycles, despite the test equipment having a high current and Ah-counting accuracy. To minimise the drift during cycling in the 10% SOC intervals, a combination of Ah-counting and an in-house developed voltage control method was used [21]. The voltage control method did not only successfully maintain the SOC interval, but could also indicate if a cell had experienced faster ageing than expected and was in need of an extra reference performance test (RPT).

The method tracks the voltage maximum and minimum at the end of each charge and discharge cycle, together with Ah-counting. The first cycle is an initiation or control cycle with a CC discharge and charge using Ah-counting, where the end voltage values is stored as two control variables. After each charge and discharge the end voltage is compared to the voltage from the control cycle according to

$$\Delta V = \left| V_{upper/lower,1} - V_{upper/lower,n} \right| < V_{limit}. \quad (1)$$

If ΔV is within a predetermined limit value, V_{limit}, the cycling proceeds. If not, a correction cycle of CC-constant voltage (CV) charging is performed to the OCV for the upper SOC level. The next cycle then becomes the new control cycle. Maximum 10% of the cycles were allowed to be control cycles, if exceeded, the test was aborted. V_{limit} was adjusted with respect to the C-rate, SOC and resistance to ensure a deviation of max 1% SOC [21].

When testing at 80–90% SOC, two different methods were used; plain CC and CC-CV charging. Using the first method, the cells were cycled with Ah-counting in combination with the voltage control method described above and in Ref. [21]. However, charging using CC at this high SOC level result in reaching voltages above the maximum 4.15 V. A maximum upper safety voltage of 4.25 V was used, and the lifetime tests were terminated when the charge voltage reached this level. For the second method, the CV charging occurred at 4.06 V, corresponding to 90% SOC.

For the wider SOC intervals CC-CV charging at the 90% SOC OCV of 4.06 V was used. For the cells tested in 0–90% SOC, 2.8 V were used as 0% SOC, while the tests conducted in 10–90% SOC used Ah-counting to determine the 10% SOC level.

In order to compare the cycle life from the different sizes of SOC intervals in the test matrix, the number of full cycle equivalents (FCEs) were used. These are here defined as the total discharge current throughput over the rated cell capacity, Q_{rated}, as

$$FCE = \frac{\int i_{dch}(t)dt}{Q_{rated}} \quad (2)$$

For these cells, Q_{rated} is equal to 26 Ah.

The capacity and resistance were measured using RPTs at 25 °C. The total capacity is defined as the 1C discharge capacity measured in the range 4.15–2.8 V. The resistance was calculated as the quota of the voltage and current differences taken prior and after a 10 s 5 C discharge pulse at 50% SOC according to

$$R = \frac{V_{0\ s} - V_{10\ s}}{I_{0\ s} - I_{10\ s}} \quad (3)$$

The capacity and resistance from the initial RPT were used to present the normalised capacity retention, $\frac{Q_{cell}}{Q^0_{cell}}$, and resistance increase, $\frac{R_{cell}}{R^0_{cell}} - 1$.

For the first 500–600 FCEs RPT were conducted every 100 FCEs, and after that approximately every 200 FCEs. For tests with slow ageing the RPTs were performed with much lower frequency, up to 1000 FCEs between the RPTs.

3. Analysis methods

The cell OCV curve is the result of the potential difference of the positive (PE) and negative electrode (NE) according to

$$V_{cell} = V_{PE} - V_{NE} \quad (4)$$

where the electrode voltage is related to the degree of lithiation of the material. As the cell ages, changes can be seen in the OCV [13]. By using cell voltage curve fitting analysis, the ageing can be quantified by tracking this change in the OCV. Such analysis can quantify and distinguish between degradation modes and results in an estimation of the three most commonly reported degradation modes; loss of lithium inventory (LLI), loss of active material on the PE (LAM_{PE}) and NE (LAM_{NE}), respectively [18].

The degradation modes can be linked to different ageing mechanisms that contributes to capacity and power fade:

- LLI is a result of Li-ions being consumed by parasitic reactions and are no longer available to be cycled between the PE and NE. These parasitic reactions are different decomposition reactions, lithium plating, formation of solid electrolyte interphase (SEI) or cathode electrolyte interphase (CEI). Li-ions trapped in isolated active material also give rise to LLI.
- LAM_{PE} corresponds to PE material that is no longer available for insertion of Li-ions due to structural disordering, particle cracking or loss of electric contact.

- LAM_{NE} is NE material that is no longer available for Li-ion insertion due to particle cracking, blocking of reaction sites by resistive film formation or loss of electric contact [18].

To be able to analyse the ageing mechanisms, galvanostatic measurements with C/10 or slower on both full-cell and half-cell are required to minimise any overpotential. The cell voltage at a given discharge capacity (Q_{cell} Ah) can then be calculated as

$$V_{cell}(Q_{cell}) = V_{PE}(Q_{PE}) - V_{NE}(Q_{NE}) \tag{5}$$

where $V_{PE}(Q_{PE})$ and $V_{NE}(Q_{NE})$ are the electrode potentials at cell capacity Q_{cell}. The electrode capacity is described by the measured half-cell capacity $q_{PE/NE}$ and a scaling factor $S_{PE/NE}$

$$Q_{PE} = q_{PE}S_{PE} \tag{6}$$

$$Q_{NE} = q_{NE}S_{NE} \tag{7}$$

To relate the half-cell electrode capacities to Q_{cell}, a shift of $\sigma_{PE/NE}$ in relation to the full-cell needs to be introduced:

$$Q_{cell} = Q_{PE} + \sigma_{PE} = q_{PE}S_{PE} + \sigma_{PE} \tag{8}$$

$$Q_{cell} = Q_{NE} + \sigma_{NE} = q_{NE}S_{NE} + \sigma_{NE} \tag{9}$$

Substituting (8) and (9) into (5) gives the equation for the voltage curve fit:

$$V_{cell}(Q_{cell}) = V_{PE}(Q_{cell} - \sigma_{PE}) - V_{NE}(Q_{cell} - \sigma_{NE}) \tag{10}$$

A visualisation of $q_{PE/NE}$, $S_{PE/NE}$, and $\sigma_{PE/NE}$ in relation to the cell capacity and potential can be seen in Fig. 1a. Comparing the changes in estimated parameters between the fresh and the aged cells enables categorisation and quantification of the cell ageing due to LAM and LLI.

The LAM is directly proportional to the respective scaling factor for the electrodes. To quantify the ageing related to the different cycling protocols and conditions, the ageing associated with the formation process needs to be subtracted. As this analysis is performed on commercial cells that has been treated by the manufacturer, the first measured C/10

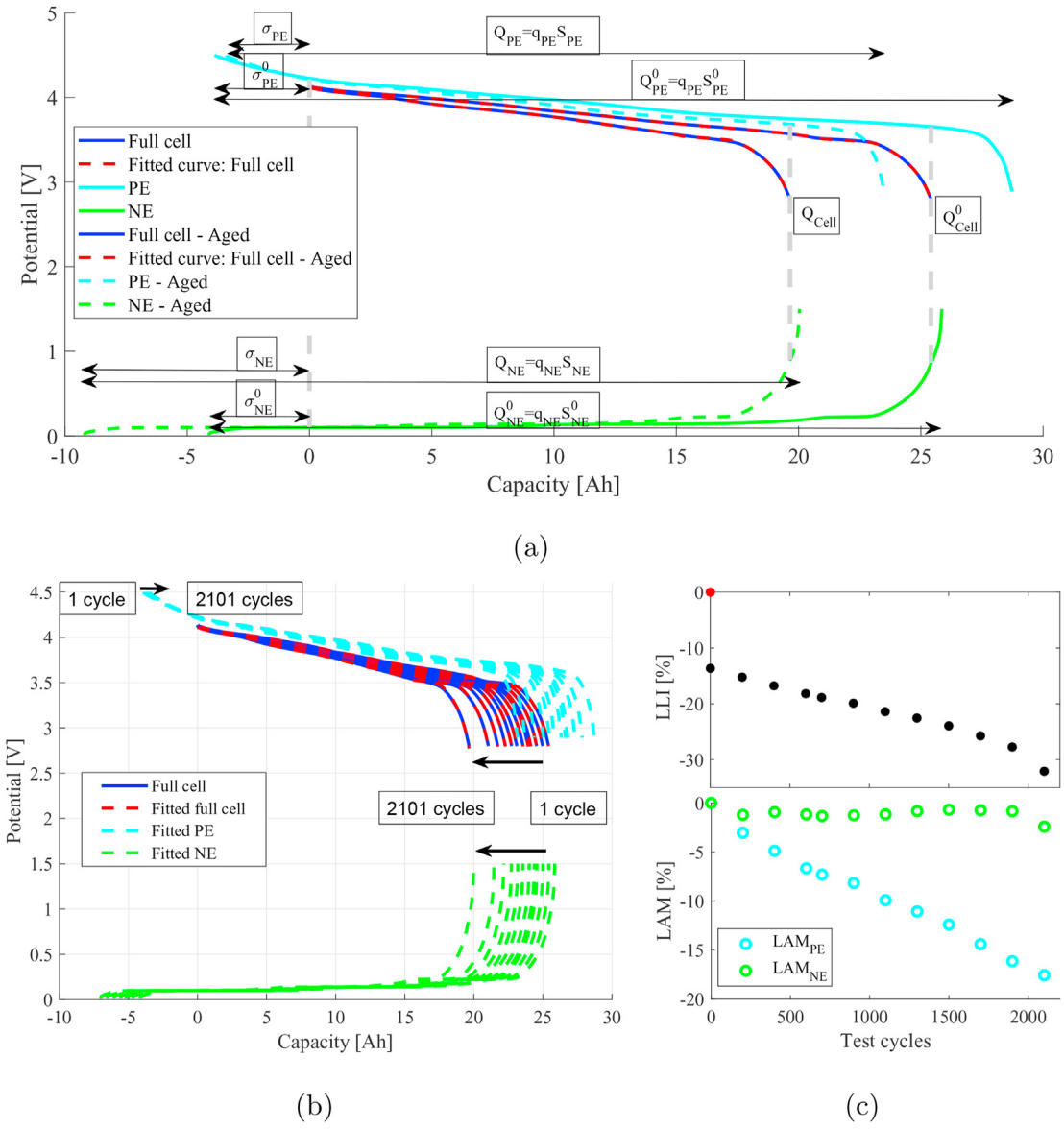

Fig. 1. (a) Visualisation of the estimation parameters for initial to aged stage. The superscript 0 denotes the first cycle. (b) Measured and estimated potential for the cell tested in 10–90% SOC at 45 °C. (c) Estimation of LAM_{PE}, LAM_{NE} and LLI for each C/10 discharge cycle. The red dot indicates the assumed 0% LLI just after cell assembly, prior to the formation process. (For interpretation of the references to colour in this figure legend, the reader is referred to the Web version of this article.)

cycle is used as a reference to calculate the LAM according to

$$LAM_{PE} = \frac{S^0_{PE} - S_{PE}}{S^0_{PE}} \tag{11}$$

$$LAM_{NE} = \frac{S^0_{NE} - S_{NE}}{S^0_{NE}} \tag{12}$$

The LLI is the amount of Li that is not re-intercalated in the PE during discharge. It is estimated based on the state-of-lithiation (SOL) of the PE at end of discharge (EOD). During the formation process, Li is consumed through formation of a passivating film on the electrode materials; typically around 15% of the capacity is lost [22]. This contribution to the ageing is then subtracted, so that only the LLI due to the cycling is included in the analysis:

$$LLI = S^0_{PE} SOL^0_{PE,EOD} - S_{PE} SOL_{PE,EOD} \tag{13}$$

SOL is calculated from:

$$SOL_{PE,EOD} = \frac{Q_{cell} - \sigma_{PE}}{q_{PE} S_{PE}} \tag{14}$$

$$SOL_{NE,EOD} = 1 - \frac{Q_{cell} - \sigma_{NE}}{q_{NE} S_{NE}} \tag{15}$$

As the film-formation is a dynamic process during the battery lifetime, the above is a simplification. Nevertheless, the emerging trends give vital information on battery ageing.

One example of the analysis process is displayed for a cell tested in 10–90% SOC at 45 °C (Fig. 1b). The blue solid lines are the measured cell potentials and the red, cyan and green lines are the estimated cell and electrode potentials, using a least-square approach. This analysis was made throughout the cell's cycle-life and each C/10 cycle provides a snapshot of the current ageing.

The estimation results (Fig. 1c) show that this cell has an initial LLI of 13.6% (assuming a $SOL^{0*}_{PE} = 100\%$ SOL for the fresh cell). Over the cycle-life it is continuously experiencing LLI and at EOL (2101 cycles) it has 32.1% LLI. The LLI due to cycling is 18.5% considering the first measured C/10 cycle as the reference, $SOL^0_{PE} = 86.4\%$ SOL, hence subtracting the initial LLI.

The LAM is estimated based on the initial cycle being the reference and thereby starts at 0 for the first cycle. This is a reasonable assumption, as the formation process is unlikely to damage the active materials to any large extent. The LAM_{PE} increases continuously with cycle number, while the LAM_{NE} is very small, ~1%. It is first at EOL that a larger loss (2.7%) is seen, however, the loss is still very small compared to the 17.6% LAM_{PE}.

A few possible concerns is that the model may have more difficulties and a lower fitting accuracy for a very aged cell, since the half-cell data is measured on a fresh cell. A large resistance increase on one electrode could lead to difficulties fitting the data, despite the slow discharge. Uneven ageing among the two mixed electrode materials is another possible uncertainty.

4. Results

4.1. Lifetime cycling

For the tests conducted in 0–90% SOC intervals, Fig. 2, faster ageing at higher temperatures can be seen. The tests were conducted using +2C/-2C with CC-CV charging at the voltage corresponding to 90% SOC (4.06 V). Similar trends can be seen for the tests performed at 25 and 45 °C in 10–90% SOC with +1C/-2C.

Comparing the four cells tested in 0–90% SOC and 10–90% SOC at 25 and 45 °C, it can be noted that at 45 °C the cell with +1C charge rate ages more rapidly per FCE compared to the cell with +2C. Here, the effect of time per FCE comes into play, calendar ageing is generally faster at higher temperatures and SOC [4,19]. The cell tested in 10–90% SOC with +1C/-2C had an average cycling rate of 7.2 FCE/day, while the cell tested with 0–90% SOC with +2C/-2C had an average of 9.5 FCE/day. For the tests at 25 °C, the slower charge rate and smaller SOC interval only resulted in slightly slower ageing. This is expected, as the calendar ageing is slower at lower temperature. This effect is only seen when accounting for the capacity loss as a function of number of FCEs.

Another important observation can be made when comparing the large SOC intervals, 0–90% SOC, to the two tests using 10% SOC intervals, e.g. 80–90% SOC at 25 and 45 °C with +2C/-2C, with CC-CV at the same cutoff voltage (4.06 V). Even though the former cells mostly were charged with currents less than +2C, due to reaching 4.06 V early in the charging process, the capacity retention trend is similar to those conducted in 0–90% SOC.

After 1300 FCE, the cells tested at 45 °C diverge from each other. The cell in the large SOC interval, 0–90% SOC, experience rapid increase in the ageing, while the cell tested in 10% SOC interval did not. The cells tested at 25 °C did instead follow a similar trend in capacity retention during the full test period.

The evolution of resistance for the 7 cells differ more explicitly. The cells tested in 0–90 and 10–90% SOC show a larger resistance growth compared to the cells tested at 80–90% SOC. The smallest resistance increase can be seen for the cell tested in 80–90% SOC at 25 °C.

The tests in 10% SOC intervals at different SOC levels for +2C/-2C CC cycling are shown in Fig. 3. Interestingly, a clear discretisation in ageing

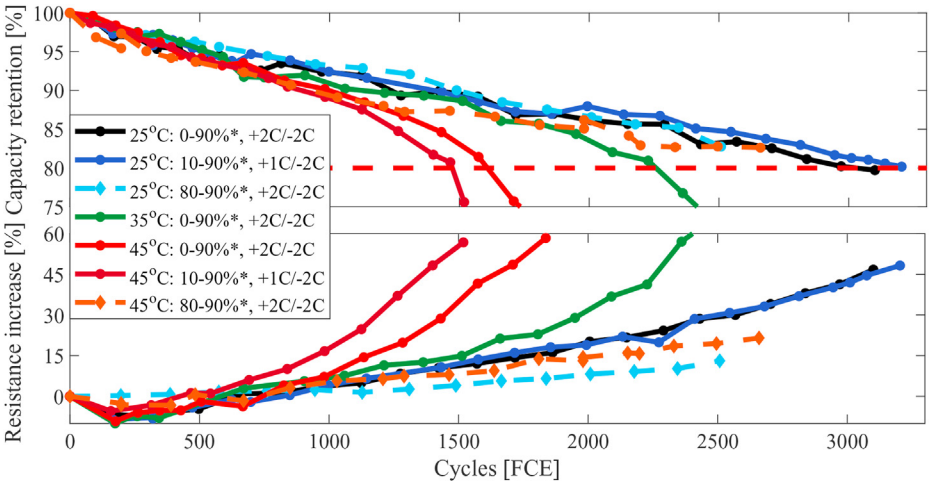

Fig. 2. Comparison of capacity retention and resistance increase for the cells tested in 0–90% SOC, 10–90% SOC and 80–90% SOC at 25 and 45 °C.

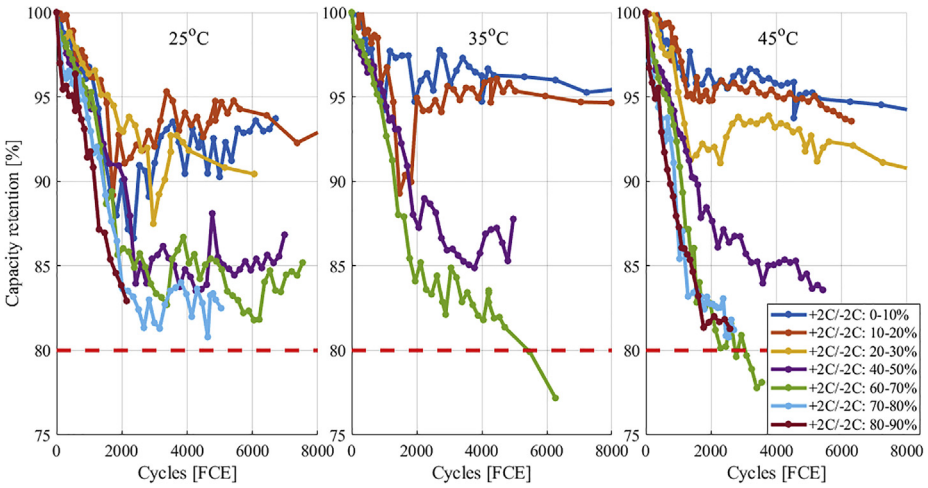

Fig. 3. Capacity retention for cells cycled in 10% SOC intervals at different SOC levels at 25, 35 and 45 °C.

could be seen with SOC interval. At 25 °C, two groups could be observed, while there were three for the two higher temperatures (40–50% SOC forming an intermediate group).

Moreover, the three lowest SOC levels, 0–10, 10–20 and 20–30% SOC, all displayed unexpected long cycle life with very slow capacity loss. While the large SOC range tests (Fig. 2) had cycle lives less than 3200 FCE, most cells are far from the EOL criteria of 80% capacity even after 8000 FCEs. The cells tested at higher SOC levels, 60–70, 70–80 and 80–90% SOC, did show an initial capacity retention comparable to the larger 0–90 and 10–90% SOC intervals, but with a slower degradation after ~2000 FCEs.

Ageing tests require long testing time and, in combination with the surprisingly slow ageing trends, most of the tests had to be terminated before reaching the set EOL criteria of 80% remaining capacity. The two tests at 80–90% SOC, where the CC was kept during the charging, had to be terminated prematurely when the maximum safety voltage of 4.25 V was reached. These cells also had slightly more gas-buildup with a completely filled gas-pocket and higher pressure compared to the cells kept below 4.15 V.

For the cells tested in small SOC intervals with different C-rates, Fig. 4, the ageing increased with C-rate. While the 1C and 2C tests at low SOC maintained 95% capacity during more than 6000 FCEs, the 4C cells aged faster, but not as fast as expected. The investigated cell was not designed for fast charging or discharging. For short pulses, 1–10 s, it should be able to deliver up to 6C. However, the 4C constant current for the long duration of 1.5 min was assumed to be detrimental to the cell.

Ageing at elevated temperatures could only be seen in high SOC intervals. At low SOC, the cells tested at 25 °C aged faster, especially at 4C. The intermediate temperature of 35 °C appeared to be the most beneficial independent of C-rate. For the intermediate SOC interval of 40–50% SOC, performed using +2C/-2C, the difference in degradation between the three temperatures was negligible.

For the cells tested with +4C/-4C at 25 °C, the resistance increase was minimal. Despite this, a rather fast capacity degradation could be seen. At

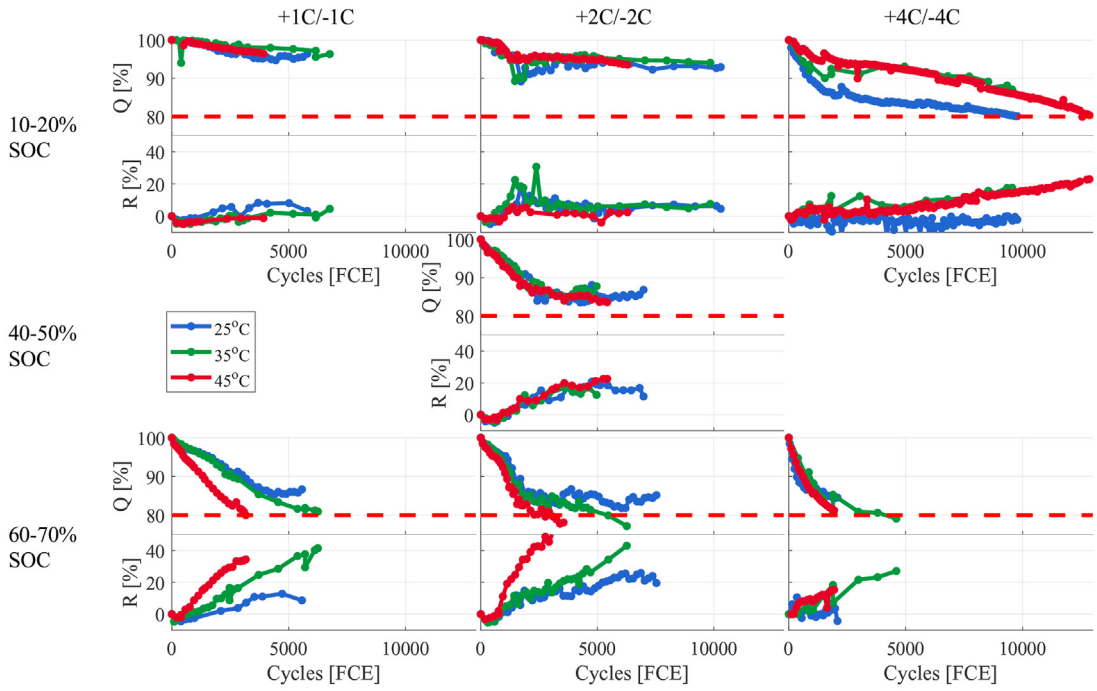

Fig. 4. Capacity retention and resistance increase for different SOC intervals for the cells tested with +1C/-1C, +2C/-2C and +4C/-4C at 25, 35 and 45 °C.

low SOC, the test at 25 °C degrades much faster than at the two higher temperatures. At the higher SOC intervals on the other hand, no clear degradation due to the increased temperature was seen. The two cells cycled at elevated temperatures (35 and 45 °C) show similar ageing trends up to 2000 FCE. For the cell tested at 35 °C, a calibration of the test equipment caused a temporary increase in the capacity when the test was resumed. These events are unavoidable, but in this case, the test could continue for a longer period, and a clear trend still noted.

4.2. Post mortem analysis

A selected number of cells were subjects to PM analysis (Table 1). The full disclosure can be found in Refs. [23–25]. The analysis included the impact of SOC, C-rate and temperature. More details on the PM analysis can be found in the Supplementary Information.

4.2.1. Impact of SOC level

When comparing the electrode materials from two cells cycled in different SOC intervals, +2C/-2C 10–20% SOC and 60–70% SOC at 45 °C, it was seen that the NE from the cell cycled in 60–70% SOC had a higher resistance compared to the NE from the cell tested in 10–20% SOC (suppl. Fig. S2). For both cells, manganese could be found in the SEI (suppl. Fig. S3). The quantity of Mn was much higher and the thickness of the SEI, estimated by hard X-ray photoelectron spectroscopy (HAXPES) [23], was thicker for the cell cycled at 60–70% SOC, indicating more side reactions.

The PM investigation concluded that the NE only had minor loss of active material, while the PE suffered from larger loss of active material. The LAM_{PE} was more severe at higher SOC. Using Incremental Capacity Analysis (ICA), it was concluded that the NMC was the origin for the LAM_{PE} (suppl. Fig. S4). This was based on the intensity decrease of the NMC peak at 3.75 V, compared to the uncycled reference cell, while the two peaks at 4.0 and 4.1 V, corresponding to LMO, remained largely unchanged [23].

4.2.2. Impact of C-rate

Moreover, analysis of Mn in the SEI suggested a slower dissolution rate at low SOC intervals when comparing a cell cycled at 10–20% SOC at +4C/-4C with a cell cycled at 60–70% SOC at +2C/-2C. Both cells were cycled at 45 °C and to 80% capacity retention.

PM analysis of two cells tested with different C-rates, 1C and 4C, in 60–70% SOC at 35°C showed that the higher C-rate caused more carbonate formation at the PE. On the other hand, greater salt degradation and formation of oxygen containing species was found on the PE after cycling at a slower C-rate (suppl. Fig. S5) [25].

4.2.3. Impact of temperature

Temperature effects were investigated for cells tested in 0–90% SOC with +2C/-2C at 25°C and 45°C. In suppl. Fig. S6 it can be seen from the remaining capacity of the individual electrodes that higher temperature leads to a larger loss of active material in the PE. Both cells also displayed smaller LAM_{NE}.

For the cell tested at higher temperature, increased salt degradation and more products relating to this, e.g. phosphorus and fluorine containing SEI species, could be found on the NE compared to the cell tested at 25°C (suppl. Fig. S7) [24,25].

4.3. Estimation of loss factors

A summary of ageing factors for the 15 tested cells included in this analysis can be seen in Fig. 5. The tested cells were cycled for different number of FCEs and different number of days. To conduct a valid comparison, the estimated ageing was normalised over the largest contributing factor to the ageing, the number of FCEs. The ageing, however, is not linear with time and the difference in number of test days (calendar ageing) has not been accounted for. Hence, the ageing contribution due to time should be larger for lower C-rate tests.

Studying the example in Fig. 1, which test was conducted over 2101 test cycles (10–90% SOC), corresponding to 1519 FCEs, the cell experienced a total LAM_{PE} of 17.6%, corresponding to 116 ppm/FCE. The 2.7%

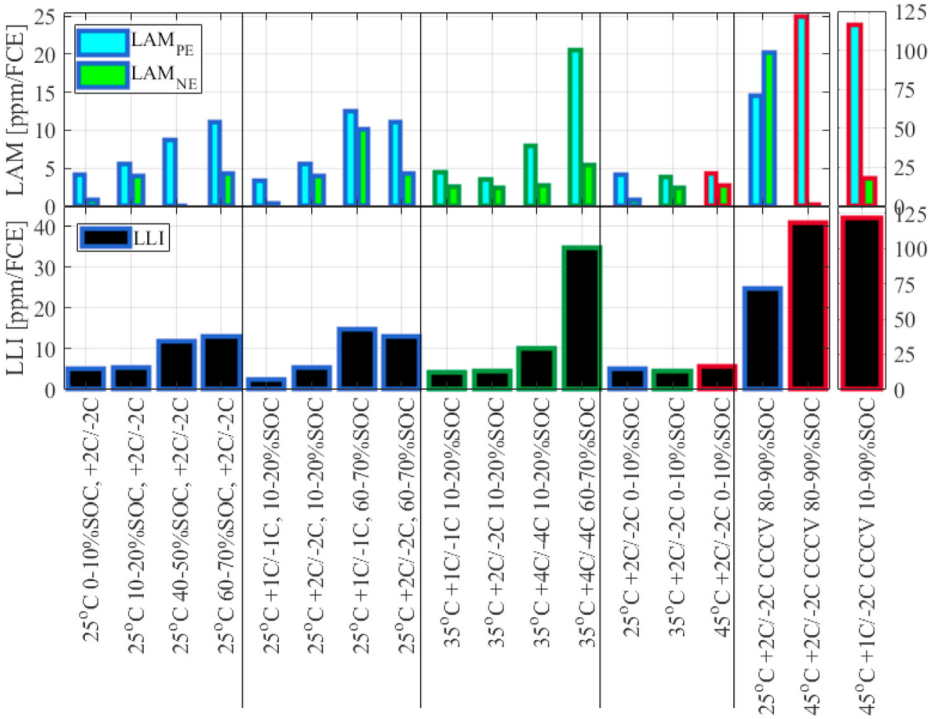

Fig. 5. Estimated LAM and LLI per FCE for 15 of the tested cells. The cell tested in 10–90% SOC had a much larger loss per FCE and a separate y-axis is therefore used. The colour of the bar's frame indicated the ambient cycling temperature: blue for 25 °C, green for 35 °C, and red for 45 °C. (For interpretation of the references to colour in this figure legend, the reader is referred to the Web version of this article.)

LAM_{NE} corresponds to 18 ppm/FCE and the 18.5% LLI to 122 ppm/FCE. The results per FCE can be seen to the right in Fig. 5, LAM_{PE} (light blue) and LAM_{NE} (light green) as well as LLI (black). The frame colour of the bar indicates the ambient cycle temperature: blue for 25 °C, green for 35 °C, and red for 45 °C. Most of the tested cells did not reach EOL, with only moderate ageing observed. Nevertheless, this analysis captured some interesting trends.

4.3.1. LAM_{PE}

The first trend seen is that higher SOC levels increase the loss of active material in the PE. This trend can most clearly be seen for the cells tested at 25 °C (first section in Fig. 5). The same phenomenon can also be seen at 35 °C, but only two SOC levels are included. High C-rate, i.e. 4C, also seems to be a contributor to increased loss of PE material.

There is also an impact of temperature for the LAM_{PE}. The PE material loss seems to be larger at 25 °C compared to 35 °C, which was not expected (the PM analysis showed larger LAM_{PE} at higher temperature). For example, of the three cells tested at 0–10% SOC with 2C at different temperatures (fourth section in Fig. 5), the cell tested at 25 °C showed the largest ageing per FCE. The PE material loss is lowest at 35 °C, but very similar to 45 °C.

4.3.2. LLI

A clear trend seen for increased C-rate (see the results at 35 °C, third section in Fig. 5) is the "slippage" of the NE, i.e. the amount of side reactions seen as LLI. The higher C-rates showed a larger slippage indicative of more side reactions. The slippage was also larger at the higher SOC levels (see first and fifth section in Fig. 5), showing increased side reactions at higher SOC levels.

The two cells tested at 80–90% SOC at 25 and 45 °C showed large LLI and higher at 45 °C. This demonstrates that high SOC and high temperature are factors that increase the LLI. Even though the cells tested with 0–10% SOC at 2C (fourth section in Fig. 5) showed very slow ageing, a weak temperature effect could possibly be the reason that the cell tested at 45 °C experienced slightly more side reactions than the cell tested at 35 °C.

4.3.3. LAM_{NE}

The LAM_{NE} was in most cases smaller than the LAM_{PE}, but the spread is larger and two trends was observed. LAM_{NE} was in most cases larger for the cells tested at high SOC. The low temperature also seemed to have a negative impact on the ageing, as seen for the cells tested with 2C in 10–20% SOC at 25 and 35 °C and the cells tested in 80–90% SOC at 25 and 45 °C. For the latter, LAM_{NE} at 25 °C is high, 20 ppm/FCE, and larger than for the cell tested in 10–90% SOC. For the cells tested at 0–10% SOC the reverse trend was observed: increased LAM_{NE} with increased temperature.

5. Discussion

The cells tested in 10 % SOC intervals below 30% SOC have remarkably long lifetimes. The degradation of these cells was initially rather rapid, but stabilise around 95% capacity. The same type of stabilisation, but at lower capacity, is evident also at higher SOC. At higher SOC (>60% SOC), C-rate, and temperature, this does not occur to the same extent. This indicates that the electrode surfaces are more effectively passivated at lower SOC and temperature. This is reasonable since, at high SOC the electrolyte is close to or outside its stability limit at both the NE and PE, i.e. the NE potential is much lower than 1 V and the PE potential≥4 V.

The PM analysis supports the above and allows for an estimation of the LLI. The PM analysis with HAXPES show that the cells tested at low SOC have a thinner SEI compared to those tested at higher SOC. Similarly, high temperature generates a larger amount of salt degradation products and other products related to a less passivating SEI. Furthermore, a clear trend in increased LLI with higher SOC levels is seen.

One reason for the good cyclability at low SOC levels could also be the mixed PE and the specific voltage interval. LMO combined with graphite prefers a voltage range of 2.8–4.15 V, while NMC vs. graphite can be used in 2.5–4.2 V. Tests with cells containing only NMC vs. graphite with 2.5 V as 0% SOC tested at 5–10% SOC have demonstrated increased ageing at low SOC [11]. Limiting the voltage window will limit the available energy, but it will also prolong the overall lifetime.

In this study, the amount of NMC is larger than the amount of LMO. As LMO is prone to Mn dissolution, it is unexpected that the large LAM_{PE} seems to be due to loss of NMC. NMC can, however, suffer from mechanical instability and structural changes in the surface, resulting in cracking of the particles and impedance increase [26]. Moreover, NMC has rather low rate capabilities due to slow lithium diffusion [27], which could explain part of the poor cycle behaviour at 4C. It is also known that the rate capability is reduced with decreasing temperature, which may explain the increased ageing rate for the 4C tests at 25 °C. Poor rate capability in the passivating films could also be the reason for the lack of resistance increase for the two cells tested at 4C at 25 °C, which could occur due to cracking of SEI or CEI.

Li-plating is another important aspect when testing at high C-rate. The probability for Li-plating is highest when charging at low temperature and at high SOC with high C-rate. However, as no sign of Li-plating could be seen in the voltage response during cycling and considering that the highest charge level only was 70% SOC, breakdown of the SEI seems to be a more likely scenario for the low resistance.

The accelerated ageing at high SOC is likely also an effect of the cross-talk between the electrode materials. In the PM analysis, Mn was found in the SEI and to a larger extent in the cell tested in high SOC, indicating that Mn dissolution from LMO or NMC, or both, occurs. Mn dissolution most likely originates from the LMO, as the onset voltage for dissolution is around 4 V [28]. The higher LAM_{PE} seen at higher SOC and temperature could be a result of increased instability of the PE under these conditions. The PM analysis also revealed increased electrolyte and salt degradation at elevated temperatures. Salt degradation has previously been linked to Mn dissolution and side reactions at the PE, resulting in LAM_{PE} [27–29].

For mixed electrodes, different electrode materials are active at different cell potentials. This is a likely reason for the different ageing trends seen at different SOCs. In a study on a mixed LMO-NMC (1:1 wt%) electrode, it could be seen that the materials are delithiated and lithiated at different voltage levels [30]. Through in situ X-ray diffraction during discharge and charge, changes in the lattice parameters of the two materials were observed. In a half cell, NMC was active in the beginning of the charge process, while the LMO was active above ~3.9 V [30]. Hence, it is likely that when the LMO is activated at higher SOC levels, several new side reactions - such as Mn dissolution - are activated. It is reasonable to believe that these lead to a cross-talk where Mn and other degradation products destabilise the SEI at the NE and also cause structural instability of NMC.

For the estimation of loss factors, the model does not account for impedance contributions on the electrodes, where uneven impedance rise in the electrodes could impact the results. The data were recorded at a slow C-rate, C/10, to minimise the impedance contribution. However, if the cells experience highly uneven impedance rise in the electrodes this could possibly be seen as a false loss of active material. Based on the PM results, the impedance rise was found to be highest on the NE, which in most cases will be the limiting electrode. Large loss of NE material observed for a few test cases, in combination with high LLI, indicate a thicker SEI due to side reactions.

6. Conclusions

For the commercial LIB cells studied here, there is a clear difference in the ageing as a result of the used SOC level. Cells tested at high SOC levels show increased ageing with temperature, increased LAM_{PE} and larger LLI. For the low and middle SOC levels, the absence of a temperature

effect (25–45 °C) on the cell capacity is surprising.

The temperature do, however, show an interesting effect on the LAM_{PE} at low SOC. Unexpectedly, the LAM_{PE} is larger at 25 °C compared to 35 °C or 45 °C. At high SOC and with high temperature it becomes even larger.

The higher C-rates also impacts the LAM_{PE} negatively. The higher C-rate also lead to larger LLI, especially for high SOC levels, indicating more side reactions are taking place.

Declaration of competing interests

The authors declare that they have no known competing financial interests or personal relationships that could have appeared to influence the work reported in this paper.

Acknowledgements

Support from the Swedish Energy Agency, Swedish Electromobility Center, STandUP for Energy, Volvo car corporation, Chalmers University of Technology and Corporate Research ABB AB are gratefully acknowledged.

Appendix A. Supplementary data

Supplementary data to this article can be found online at https://doi.org/10.1016/j.powera.2021.100054.

References

[1] J. Vetter, P. Novák, M. Wagner, C. Veit, K.-C. Möller, J. Besenhard, M. Winter, M. Wohlfahrt-Mehrens, C. Vogler, A. Hammouche, Ageing mechanisms in lithium-ion batteries, J. Power Sources 147 (1–2) (2005) 269–281.

[2] R.B. Wright, C.G. Motloch, J.R. Belt, J.P. Christophersen, C.D. Ho, R.A. Richardson, I. Bloom, S.A. Jones, V.S. Battaglia, G.L. Henriksen, T. Unkelhaeuser, D. Ingersoll, H.L. Case, S.A. Rogers, R.A. Sutula, Calendar-and cycle-life studies of advanced technology development program generation 1 lithium-ion batteries, J. Power Sources 110 (2002) 445–470, https://doi.org/10.1016/S0378-7753(02)00210-0.

[3] V. Agubra, J. Fergus, Lithium ion battery anode aging mechanisms, Materials 6 (4) (2013) 1310–1325.

[4] P. Keil, A. Jossen, Calendar aging of NCA lithium-ion batteries investigated by differential voltage analysis and coulomb tracking, J. Electrochem. Soc. 164 (1) (2016) A6066–A6074, https://doi.org/10.1149/2.0091701jes, 10.1149/2.0091701jes.

[5] P. Keil, S.F. Schuster, J. Wilhelm, J. Travi, A. Hauser, R.C. Karl, A. Jossen, Calendar aging of lithium-ion batteries: I. impact of the graphite anode on capacity fade, J. Electrochem. Soc. 163 (9) (2016) A1872–A1880, https://doi.org/10.1149/2.0411609jes. http://jes.ecsdl.org/content/163/9/A1872.full.pdf+html.

[6] Y. Ito, K. Sato, A. Tamai, K. Nakao, Unexpected relation between degradation rate of lithium ion battery and stage structure of graphite anode, Meet. Abstr. MA2018–02 (4) (2018) 216. http://ma.ecsdl.org/content/MA2018-02/4/216.abstract.

[7] J. Groot, State-of-Health Estimation of Li-Ion Batteries: Cycle Life Test Methods, Licentiate Thesis, 2012.

[8] S. Käbitz, J.B. Gerschler, M. Ecker, Y. Yurdagel, B. Emmermacher, D. André, T. Mitsch, D.U. Sauer, Cycle and calendar life study of a graphite|LiNi1/3Mn1/3Co1/3O2 Li-ion high energy system. Part A: full cell characterization, J. Power Sources 239 (2013) 572–583, https://doi.org/10.1016/j.jpowsour.2013.03.045. http://www.sciencedirect.com/science/article/pii/S0378775313004369.

[9] M. Ecker, N. Nieto, S. Käbitz, J. Schmalstieg, H. Blanke, A. Warnecke, D.U. Sauer, Calendar and cycle life study of Li(NiMnCo)O2-based 18650 lithium-ion batteries, J. Power Sources 248 (2014) 839–851, https://doi.org/10.1016/j.jpowsour.2013.09.143. http://www.sciencedirect.com/science/article/pii/S0378775313016510.

[10] J. Groot, State-of-health Estimation of Li-Ion Batteries: Ageing Models, Ph.D. thesis, Chalmers University of Technology, 2014.

[11] J. Schmalstieg, S. Käbitz, M. Ecker, D.U. Sauer, From accelerated aging tests to a lifetime prediction model: analyzing lithium-ion batteries, in: 2013 World Electric Vehicle Symposium and Exhibition (EVS27), 2013, pp. 1–12, https://doi.org/10.1109/EVS.2013.6914753.

[12] T. Waldmann, A. Iturrondobeitia, M. Kasper, N. Ghanbari, F. Aguesse, E. Bekaert, L. Daniel, S. Genies, I.J. Gordon, M.W. Löble, E. De Vito, M. Wohlfahrt-Mehrens, Review—post-mortem analysis of aged lithium-ion batteries: disassembly methodology and physico-chemical analysis techniques, J. Electrochem. Soc. 163 (10) (2016) A2149–A2164, https://doi.org/10.1149/2.1211609jes. http://jes.ecsdl.org/content/163/10/A2149.full.pdf+html.

[13] I. Bloom, A.N. Jansen, D.P. Abraham, J. Knuth, S.A. Jones, V.S. Battaglia, G.L. Henriksen, Differential voltage analyses of high-power, lithium-ion cells: 1. technique and application, J. Power Sources 139 (1) (2005) 295–303, https://doi.org/10.1016/j.jpowsour.2004.07.021.

[14] K. Honkura, K. Takahashi, T. Horiba, Capacity-fading prediction of lithium-ion batteries based on discharge curves analysis, J. Power Sources 196 (23) (2011) 10141–10147, https://doi.org/10.1016/j.jpowsour.2011.08.020.

[15] M. Dubarry, C. Truchot, B.Y. Liaw, Synthesize battery degradation modes via a diagnostic and prognostic model, J. Power Sources 219 (2012) 204–216, https://doi.org/10.1016/j.jpowsour.2012.07.016.

[16] P. Svens, R. Eriksson, J. Hansson, M. Behm, T. Gustafsson, G. Lindbergh, Analysis of aging of commercial composite metal oxide – li4ti5o12 battery cells, J. Power Sources 270 (2014) 131–141, https://doi.org/10.1016/j.jpowsour.2014.07.050.

[17] A.S. Mussa, M. Klett, M. Behm, G. Lindbergh, R.W. Lindström, Fast-charging to a partial state of charge in lithium-ion batteries: a comparative ageing study, Journal of Energy Storage 13 (2017) 325–333, https://doi.org/10.1016/j.est.2017.07.004.

[18] C.R. Birkl, M.R. Roberts, E. McTurk, P.G. Bruce, D.A. Howey, Degradation diagnostics for lithium ion cells, J. Power Sources 341 (2017) 373–386, https://doi.org/10.1016/j.jpowsour.2016.12.011.

[19] E. Wikner, Lithium Ion Battery Aging: Battery Lifetime Testing and Physics-Based Modeling for Electric Vehicle Applications, Licentiate Thesis, 2017. https://research.chalmers.se/publication/249356.

[20] E. Wikner, Ageing in Commercial Li-Ion Batteries: Lifetime Testing and Modelling for Electrified Vehicle Applications, Ph.D. thesis, Chalmers University of Technology, 2019, https://research.chalmers.se/publication/512004.

[21] E. Wikner, J. Lesser, T. Thiringer, Accelerated lifetime testing in small soc intervals on commercial pouch cells; challenges and countermeasures, in: 2017 19th European Conference on Power Electronics and Applications (EPE'17 ECCE Europe), 2017, pp. 1–7, https://doi.org/10.23919/EPE17ECCEEurope.2017.8099133.

[22] M.R. Palacín, Understanding ageing in li-ion batteries: a chemical issue, Chem. Soc. Rev. 47 (2018) 4924–4933, https://doi.org/10.1039/C7CS00889A, 10.1039/C7CS00889A.

[23] E. Björklund, E. Wikner, R. Younesi, D. Brandell, K. Edström, Influence of state-of-charge in commercial LiNi0.33Mn0.33Co0.33O2/LiMn2O4-graphite cells analyzed by synchrotron-based photoelectron spectroscopy, Journal of Energy Storage 15 (2018) 172–180, https://doi.org/10.1016/j.est.2017.11.010.

[24] E. Björklund, Avoiding Ageing: Surface Degradation of Commercial Electrode Materials in Lithium-Ion Batteries, Ph.D. thesis, Uppsala University, Structural Chemistry, 2019.

[25] J. Scheers, E. Wikner, E. Björklund, A. Jedenmalm, A. Andersson, L. Migas, T. Thiringer, D. Brandell, Ageing Mechanisms & How to Prolong Battery Life in Vehicle and Energy Storage Applications, Final Report of STEM Project 37725-1, 2019. http://www.energimyndigheten.se/forskning-och-innovation/projektdatabas/sokresultat/GetDocument/?id=f52a66a5-22de-41e0-8a5e-e86c8f24686c&documentName=Slutrapport_37725-1_190412.pdf.

[26] R. Xu, H. Sun, L.S. de Vasconcelos, K. Zhao, Mechanical and structural degradation of LiNixMnyCozO2 cathode in Li-ion batteries: an experimental study, J. Electrochem. Soc. 164 (13) (2017) A3333–A3341. http://jes.ecsdl.org/content/164/13/A3333.full.pdf+html.

[27] I. Buchberger, S. Seidlmayer, A. Pokharel, M. Piana, J. Hattendorff, P. Kudejova, R. Gilles, H.A. Gasteiger, Aging analysis of graphite/LiNi1/3Mn1/3Co1/3O2 cells using XRD, PGAA, and AC impedance, J. Electrochem. Soc. 162 (14) (2015) A2737–A2746, https://doi.org/10.1149/2.0721514jes. http://jes.ecsdl.org/content/162/14/A2737.full.pdf+html.

[28] A. Bhandari, J. Bhattacharya, Review—manganese dissolution from spinel cathode: few unanswered questions, J. Electrochem. Soc. 164 (2) (2017) A106–A127. http://jes.ecsdl.org/content/164/2/A106.full.pdf+html.

[29] X. Lin, J. Park, L. Liu, Y. Lee, A.M. Sastry, W. Lu, A comprehensive capacity fade model and analysis for li-ion batteries, J. Electrochem. Soc. 160 (10) (2013) A1701–A1710. http://jes.ecsdl.org/content/160/10/A1701.full.pdf+html.

[30] K.-W. Nam, W.-S. Yoon, H. Shin, K.Y. Chung, S. Choi, X.-Q. Yang, In situ x-ray diffraction studies of mixed limn2o4–lini1/3co1/3mn1/3o2 composite cathode in li-ion cells during charge–discharge cycling, J. Power Sources 192 (2) (2009) 652–659, https://doi.org/10.1016/j.jpowsour.2009.02.088.